Altered ER–mitochondria contact impacts mitochondria calcium homeostasis and contributes to neurodegeneration in vivo in disease models

Kyu-Sun Lee[a,b,c,d,1], Sungun Huh[a,b,c,1], Seongsoo Lee[a,b,c,d,e,1], Zhihao Wu[a,b,c], Ae-Kyeong Kim[d], Ha-Young Kang[e], and Bingwei Lu[a,b,c,2]

[a]Department of Pathology, Stanford University School of Medicine, Stanford, CA 94305; [b]Program of Neuroscience, Stanford University School of Medicine, Stanford, CA 94305; [c]Program of Cancer Biology, Stanford University School of Medicine, Stanford, CA 94305; [d]BioNanotechnology Research Center, Korea Research Institute of Biotechnology and Bioscience, 34141 Daejeon, Korea; and [e]Gwangju Center, Korea Basic Science Institute, 61186 Gwangju, Korea

Edited by Gyorgy Hajnoczky, Thomas Jefferson University, Philadelphia, PA, and accepted by Editorial Board Member David E. Clapham August 6, 2018 (received for review December 5, 2017)

Calcium (Ca^{2+}) homeostasis is essential for neuronal function and survival. Altered Ca^{2+} homeostasis has been consistently observed in neurological diseases. How Ca^{2+} homeostasis is achieved in various cellular compartments of disease-relevant cell types is not well understood. Here we show in *Drosophila* Parkinson's disease (PD) models that Ca^{2+} transport from the endoplasmic reticulum (ER) to mitochondria through the ER–mitochondria contact site (ERMCS) critically regulates mitochondrial Ca^{2+} (mito-Ca^{2+}) homeostasis in dopaminergic (DA) neurons, and that the PD-associated PINK1 protein modulates this process. In *PINK1* mutant DA neurons, the ERMCS is strengthened and mito-Ca^{2+} level is elevated, resulting in mitochondrial enlargement and neuronal death. Miro, a well-characterized component of the mitochondrial trafficking machinery, mediates the effects of PINK1 on mito-Ca^{2+} and mitochondrial morphology, apparently in a transport-independent manner. Miro overexpression mimics *PINK1* loss-of-function effect, whereas inhibition of Miro or components of the ERMCS, or pharmacological modulation of ERMCS function, rescued *PINK1* mutant phenotypes. Mito-Ca^{2+} homeostasis is also altered in the LRRK2-G2019S model of PD and the PAR-1/MARK model of neurodegeneration, and genetic or pharmacological restoration of mito-Ca^{2+} level is beneficial in these models. Our results highlight the importance of mito-Ca^{2+} homeostasis maintained by Miro and the ERMCS to mitochondrial physiology and neuronal integrity. Targeting this mito-Ca^{2+} homeostasis pathway holds promise for a therapeutic strategy for neurodegenerative diseases.

ER–mitochondria contact site | calcium homeostasis | PINK1 | Miro | Parkinson's disease

Mitochondria are important for many aspects of cellular function, from energy metabolism and redox balance to apoptosis. Mitochondrial dysfunction has been broadly linked to diseases (1). Mitochondrial function and Ca^{2+} signaling have been intimately linked. Ca^{2+} uptake by mitochondria helps buffer cytosolic Ca^{2+} transients generated by neuronal activation, protecting from the detrimental effects of bursts of Ca^{2+} elevations. Under basal conditions, Ca^{2+} entry into mitochondria is needed for normal physiology, as mito-Ca^{2+} positively regulates the activities of TCA cycle enzymes and electron transport chain components. In a number of disease conditions, including neurodegenerative diseases such as Alzheimer's disease (AD), Huntington's disease, and Parkinson's disease, Ca^{2+} dyshomeostasis has been observed (2), and cell type-specific difference in Ca^{2+} channel activities and the ensuing homeostatic Ca^{2+} stress have been invoked to explain selective neuronal vulnerability in disease (3). The mechanism of how Ca^{2+} homeostasis is achieved in disease-relevant cell types and how it is perturbed in disease conditions is poorly understood.

AD is the most common neurodegenerative disorder and the leading cause of dementia in the elderly. Although amyloid plaques and neurofibrillary tangles are the pathological hallmarks of the disease and targets of therapeutic intervention, the recent failures of clinical trials of amyloid- and tangle-modifying therapeutics suggest that other features of the disease warrant consideration. Mitochondrial dysfunction, Ca^{2+} dyshomeostasis, altered lipid metabolism, and neuroinflammation have been observed before the appearance of plaques and/or tangles and frank neurodegeneration in the disease process (4). Recent studies have drawn attention to endoplasmic reticulum (ER)–mitochondria interaction in AD pathogenesis (5–7). Increased contacts between ER and mitochondria and associated cellular function, including lipid and Ca^{2+} transport, have been observed in AD (4). How altered ER–mitochondria signaling arises in the disease process and its contribution to disease pathogenesis in intact animals remain to be addressed.

PD is the most common movement disorder associated with rather selective degeneration of dopaminergic (DA) neurons. The molecular basis of the subtype-selective neuronal vulnerability is of major interest. The autonomous pacemaking activities

Significance

Ca^{2+} regulates cellular metabolism, proliferation, and differentiation. Ca^{2+} homeostasis is critical for cellular function and health. Mitochondria help buffer transient Ca^{2+} elevations and prevent cell death induced by Ca^{2+} overload. Mito-Ca^{2+} is also required for optimal activity of certain key mitochondrial functions, such as oxidative phosphorylation and metabolism. Thus, mito-Ca^{2+} homeostasis assumes central roles in cellular health. Endoplasmic reticulum (ER) and mitochondria make intimate contacts and exchange molecules such as Ca^{2+} and lipids. We find that ER-to-mitochondria Ca^{2+} transfer is important for mito-Ca^{2+} homeostasis and that the conserved Miro protein is critically involved. We show that mito-Ca^{2+} homeostasis is disrupted in neurodegenerative disease models and its restoration is beneficial. Our findings have important implications for therapeutic intervention of neurodegenerative diseases.

Author contributions: K.-S.L., S.H., S.L., and B.L. designed research; K.-S.L., S.H., S.L., Z.W., A.-K.K., H.-Y.K., and B.L. performed research; K.-S.L. contributed new reagents/analytic tools; K.-S.L., S.H., S.L., and B.L. analyzed data; and K.-S.L., S.H., S.L., and B.L. wrote the paper.

The authors declare no conflict of interest.

This article is a PNAS Direct Submission. G.H. is a guest editor invited by the Editorial Board.

[1]K.-S.L., S.H., and S.L. contributed equally to this work.

[2]To whom correspondence should be addressed. Email: bingwei@stanford.edu.

This article contains supporting information online at www.pnas.org/lookup/suppl/doi:10.1073/pnas.1721136115/-/DCSupplemental.

Published online September 5, 2018.

of DA neurons in disease-susceptible regions might impose higher demand for Ca^{2+} handling abilities, making these neurons particularly vulnerable to Ca^{2+} dyshomeostasis. Alteration of Ca^{2+} homeostasis has been linked to some of the disease gene products. For example, PINK1 and Parkin have been implicated in mito-Ca^{2+} homeostasis, although their modes of action are poorly understood and subjected to considerable controversy (8, 9). In vivo studies in animal models are needed to resolve these controversies.

Ca^{2+} uptake by mitochondria occurs at the ER–mitochondria contact sites (ERMCSs), where local Ca^{2+} can reach high levels (10). Proteins localized to ERMCSs include those mediating Ca^{2+} transfer, such as inositol 1,4,5-trisphosphate receptor (IP3R) at the ER, voltage-dependent anion-selective channel (VDAC) at the mitochondrial outer membrane (MOM), and mitochondrial Ca^{2+} uniporter (MCU) at the mitochondrial inner membrane (MIM) (11). Despite the importance of the ERMCS to fundamental cellular functions and its potential link to disease, its regulation and function in normal development and disease processes at the organismal level remain untested. Recent studies revealed the role of Miro, a MOM protein containing two GTPase domains and two Ca^{2+}-sensing EF hand domains (12), in ERMCS regulation (13). Miro is best known for its role in axonal transport of mitochondria, whereby it forms a multiprotein complex with Milton and Kinesin heavy chain (Khc) (14, 15). But yeast Miro was shown to localize to regions of ER–mitochondria association (16), and Miro performs a non-canonical role in regulating mito-Ca^{2+} levels in *Drosophila* and mammalian neural stem cells (NSCs) (13). How mito-Ca^{2+} homeostasis is regulated in the disease-relevant neuronal tissues remains to be determined. The goal of this study is to test whether mito-Ca^{2+} homeostasis regulated by ERMCSs is critical in the context of neurodegeneration in animal models.

Results

Mito-Ca^{2+} Level Is Elevated in the DA Neurons of Fly PD Models. We used the genetically encoded Ca^{2+} indicator mito-GCaMP (17) and the *UAS-Gal4* system to monitor mito-Ca^{2+} levels in different cell types and tissues in *Drosophila* (13). To specifically examine DA neurons, we used *TH-Gal4* to drive *UAS-mito-GCaMP* transgene expression. Punctate fluorescent signals in neuronal cell body and processes were readily detectable in larval and adult fly brains. To verify that the fluorescent reporter responds to cellular Ca^{2+} levels, we fed animals with food containing $CaCl_2$ or the Ca^{2+} chelator BAPTA and saw enhanced or diminished signals when animals were treated with $CaCl_2$ or

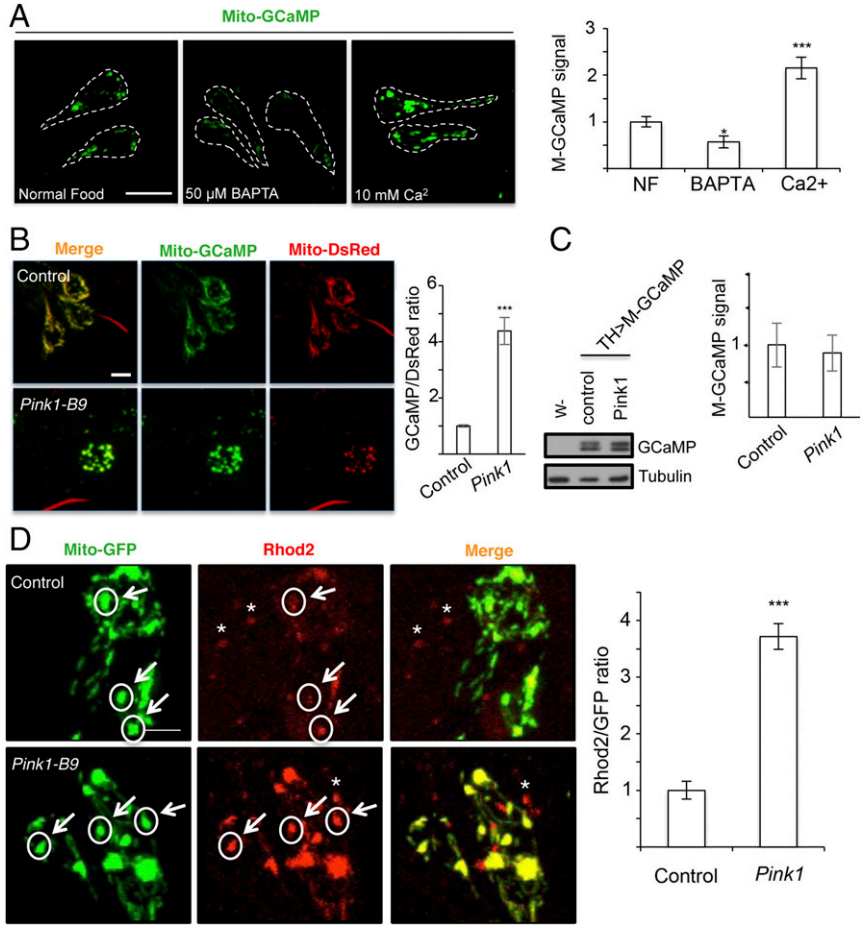

Fig. 1. Mito-Ca^{2+} analysis in DA neurons of PD model flies. (*A*) Mito-GCaMP signals in central brain DA neurons (outlined with dashed line) of third instar larvae grown on normal food or food containing BAPTA or Ca^{2+}. Quantification of relative GCaMP signal is shown in bar graph. (*B* and *C*) Images of Mito-GCaMP signals and quantification showing elevated mito-Ca^{2+} in *PINK1*^{B9} adult DA neurons. Bar graph shows mito-GCaMP signal normalized with mito-DsRed, which measures mitochondrial mass. WB in *C* shows mito-GCaMP protein level detected with anti-calmodulin antibody. (*D*) Rhod2-AM staining of mito-Ca^{2+} in *PINK1*^{B9} adult DA neurons, with mitochondria labeled by mito-GFP. Bar graph shows Rhod2-AM signal normalized with mito-GFP, which measures mitochondrial mass. Arrows and circles mark mitochondrial units with similar mass. * marks Rhod2-AM signal in non-TH^{+} neurons. Error bar: SEM; *$P < 0.05$, ***$P < 0.001$ versus control in one-way ANOVA. $n = 5$. (Scale bars in *A*, *B*, and *D*: 10 μm.)

BAPTA, respectively (Fig. 1*A*). Acute treatment by soaking larvae in PBS containing $CaCl_2$ or BAPTA for 15–20 min had similar effects. Moreover, when mitochondrial membrane potential (MMP), the driving force of mito-Ca^{2+} uptake, was depleted by the protonophore CCCP, mito-GCaMP fluorescent signals were greatly reduced (*SI Appendix*, Fig. S1*A*). Although CCCP can affect cellular pH when used at higher concentrations, at lower CCCP concentration (2 μM) and after only a 10 min treatment, when cytosolic pH was not affected, mito-GCaMP signal was still reduced (*SI Appendix*, Fig. S1 *B* and *C*). Such a CCCP treatment regimen should not significantly affect mito-GCaMP fluorescence by altering mitochondrial pH, since even at higher CCCP concentration (20 μM) and after a 1-h treatment, mitochondrial pH changed from 7.8 to 7.0 (18), which is still within the optimal range for mito-GCaMP (19). Similarly, treatment with the mitochondrial electron transport chain toxin Antimycin A, which has been shown to depolarize MMP (20), also led to reduced mito-GCaMP signals (*SI Appendix*, Fig. S1*D*). Thus, two different MMP-reducing regimens both attenuated mito-GCaMP signals, supporting the notion that the mito-GCaMP reporter is faithfully monitoring mito-Ca^{2+} levels.

We next expressed the mito-GCaMP reporter in DA neurons of *PINK1* mutant (*PINK1*^{B9}). Compared with control animals, *PINK1* mutant exhibited significantly elevated mito-GCaMP signals in central brain DA neurons (Fig. 1*B*). This difference in mito-GCaMP signal was not due to a difference in the mitochondrial mass in the imaged area, as we normalized the mito-GCaMP signal with a mito-DsRed reporter that measures mitochondrial mass (Fig. 1*B*). Neither was the difference in signal due to differential mito-GCaMP expression, as the GCaMP protein level was comparable (Fig. 1*C*). Moreover, the increase in mito-GCaMP signal in *PINK1* mutant DA neurons was not due to increased cytoplasmic Ca^{2+}, as our measurement of cytosolic Ca^{2+} signal with a cyto-GCaMP reporter, which also responded to exogenous $CaCl_2$ or BAPTA (*SI Appendix*, Fig. S2*A*), did not reveal a significant difference (*SI Appendix*, Fig. S2 *B* and *C*). We note that while cyto-GCaMP runs as a single band on Western blot (WB), mito-GCaMP runs as a doublet, presumably representing the unprocessed preprotein and the mature form. The mito-GCaMP doublets appeared in purified mitochondria at a similar ratio to the total lysate, and the lower band was more enriched in the matrix (*SI Appendix*, Fig. S2*D*). Mito-GCaMP may be translated on MOM and cotranslationally imported into mitochondria, as shown for other nuclear-encoded mitochondrial proteins (21). Mature mito-GCaMP mainly exists in the matrix, with some in the intermembrane space, and thus is usable for detecting mito-Ca^{2+}. Indeed, the mito-GCaMP signal was largely overlapping with mito-DsRed (Fig. 1*B*), whereas cyto-GCaMP was uniformly distributed in the cell (*SI Appendix*, Fig. S2 *A* and *B*).

Elevation of the mito-Ca^{2+} level in *PINK1* mutant DA neurons was independently verified by staining with Rhod2-AM (Fig. 1*D*), a Ca^{2+}-sensitive fluorescent dye that has been shown to preferentially monitor mito-Ca^{2+} in fly neurons (13, 14). Again, the difference in Rhod2-AM signal was not due to difference in the mitochondrial mass in the imaged area as we normalized Rhod2-AM signal with a mito-GFP reporter for mitochondrial mass (Fig. 1*D*). Moreover, when we induced mitochondrial enlargement by inhibiting Drp1 genetically with Drp1-DN or pharmacologically with mDivi-1, which was previously shown to cause excessive enlargement when fed to flies (22), we did not observe the same elevation of mito-GCaMP signal as in *PINK1* mutant (*SI Appendix*, Fig. S3 *A* and *B*), further demonstrating that mitochondrial enlargement alone cannot account for the observed mito-GCaMP fluorescence elevation. Collectively, these results indicate that mito-Ca^{2+} homeostasis in DA neurons is regulated by PINK1 in vivo.

In our Ca^{2+} imaging experiments, we tested dissecting and imaging the adult brains in the PBS buffer or Schneider's medium, which is closer to the physiological conditions, and the results were similar (*SI Appendix*, Fig. S3*C*). We also analyzed flies raised at 25 °C (*SI Appendix*, Fig. S3*D*) or 29 °C (Fig. 1 *B*–*D*). The results were also similar. Since in later experiments we used the *UAS-Gal4* to direct RNAi of certain genes, and the *UAS-Gal4*–directed RNAi is known to be more efficient at higher temperature, the Ca^{2+} imaging studies presented from then on were done using flies raised at 29 °C. As DA neurons are known to exhibit Ca^{2+} oscillations in vivo, we tested by using time-lapse confocal microscopy whether mito-Ca^{2+} levels also exhibit dynamic changes. From the time-lapse images, we could see that within the recording period (30 s), some mitochondria showed increased or decreased mito-GCaMP signals, whereas others showed oscillation of mito-GCaMP signals in both wild-type (WT) and *PINK1* mutant DA neurons (*SI Appendix*, Fig. S3*E*). These data support the idea that mito-GCaMP can detect dynamic changes of mito-Ca^{2+} in vivo.

Next we tested whether alteration of mito-Ca^{2+} homeostasis is a general phenomenon in PD models. In the *Drosophila* model of PD generated by transgenic (Tg) expression of human LRRK2-G2019S (23), we also observed elevation of mito-Ca^{2+} as monitored with mito-GCaMP expressed in DA neurons (*SI Appendix*, Fig. S3 *A* and *B*). Together, these data support the notion that increased mito-Ca^{2+} is broadly associated with PD pathogenesis.

Miro Mediates the Elevation of Mito-Ca^{2+} in *PINK1* Mutant DA Neurons. We next sought to understand the mechanism underlying the alteration of mito-Ca^{2+} homeostasis in *PINK1* mutant. We turned to Miro, which contains Ca^{2+}-binding EF hand motifs. The Ca^{2+} binding activity of Miro has been well studied in the context of mitochondria motility regulation as a sensor of activity-induced Ca^{2+} influx (24). Recent studies revealed a transport-independent function of Miro in regulating mito-Ca^{2+} (13). Moreover, the PINK1–Parkin pathway was shown to negatively regulate Miro level in mammalian cells through ubiquitination, and endogenous Miro protein level was increased in *PINK1* mutant (25, 26).

To test whether altered Miro abundance contributes to mito-Ca^{2+} deregulation in *PINK1* mutant DA neurons, we knocked down Miro by RNAi using a well-characterized transgenic RNAi line (27). This manipulation rescued mito-Ca^{2+} level in *PINK1* mutant DA neurons as monitored by mito-GCaMP (Fig. 2*A*). The level of mito-GCaMP protein expression was not affected by Miro-RNAi (Fig. 2*B*), suggesting that the reduction of mito-GCaMP fluorescence was due to a change of mito-Ca^{2+} level rather than reporter protein expression. Using an available *dMiro* mutant allele, we showed that 50% reduction of Miro dosage also significantly reduced mito-Ca^{2+} level in *PINK1* mutant DA neurons (*SI Appendix*, Fig. S4*C*). Next, we tested whether overexpression (OE) of Miro in DA neurons is sufficient to elevate mito-Ca^{2+} level. This was indeed the case (Fig. 2*C* and *SI Appendix*, Fig. S4*D*). Note that we observed increased mito-Ca^{2+} in newly eclosed flies, before there was any obvious sign of DA neuron degeneration, which normally occurs in aged Miro-OE flies (26). These results indicated that the up-regulation of Miro protein abundance in *PINK1* mutant is responsible for the alteration of mito-Ca^{2+}. We also examined the OE of Milton, a key component of the transport machinery, but we did not observe obvious changes in mito-Ca^{2+} level (*SI Appendix*, Fig. S4 *E* and *F*), although we could detect increased Milton expression (*SI Appendix*, Fig. S4*G*). Miro regulation of mito-Ca^{2+} thus may not be dependent on mitochondrial transport.

Ca^{2+} Transfer Through ERMCSs Is Critical for Miro-Regulated Mito-Ca^{2+} Homeostasis in DA Neurons. The ER represents a major cellular source of mito-Ca^{2+}. Mito-Ca^{2+} uptake from the ER occurs at ERMCSs where Ca^{2+} can reach high levels at microdomains. Proteins localized to these contact sites include transporters

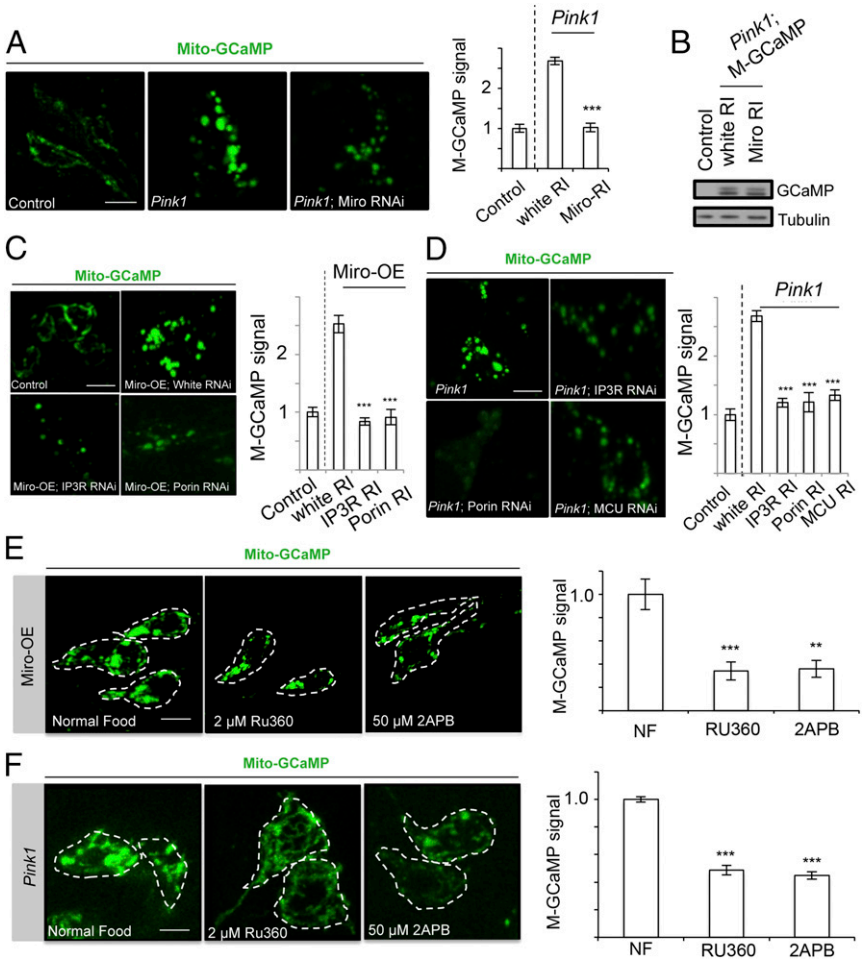

Fig. 2. Miro mediates the elevation of mito-Ca^{2+} in *PINK1*^{B9} DA neurons. (*A* and *B*) Attenuation of mito-Ca^{2+} increase in *PINK1*^{B9} adult DA neurons by Miro-RNAi. Representative images of mito-GCaMP and quantification of signal intensity are shown in *A*. Signals were normalized relative to *TH-Gal4* > *mito-GCaMP* control. WB in *B* shows comparable expression of mito-GCaMP in the genotypes analyzed. (*C* and *D*) Representative images of mito-GCaMP and quantification of signal intensity showing attenuation of elevated mito-Ca^{2+} in Miro-OE (*C*) or *PINK1*^{B9} (*D*) adult DA neurons after knocking down IP3R, Porin, and MCU. (*E* and *F*) Representative images of mito-GCaMP and quantification of signal intensity showing attenuation of mito-Ca^{2+} increase in Miro-OE (*E*) or *PINK1*^{B9} (*F*) adult DA neurons after treatment with 2 μM RU360 or 50 μM 2-APB. The DA neurons are outlined with white dashed line. Error bar: SEM; $^{**}P < 0.01$, $^{***}P < 0.001$ versus control in one-way ANOVA. $n = 5$. (Scale bars in *A* and *C*–*F*: 5 μm.)

mediating Ca^{2+} transfer, for example IP3R at the ER, VDAC at the MOM, and MCU at the MIM (11). We tested whether the ERMCS might mediate the effect of Miro on mito-Ca^{2+} dynamics. Inhibition of genes involved in Ca^{2+} transfer at the ERMCS by RNAi (*SI Appendix*, Fig. S5*A*) attenuated the aberrant mito-Ca^{2+} elevation induced by Miro-OE in DA neurons (Fig. 2*C*). Again the mito-GCaMP fluorescence change was not due to differential expression of mito-GCaMP (*SI Appendix*, Fig. S5*B*). The expression of Miro was also not affected (*SI Appendix*, Fig. S5*C*). We next tested whether ERMCS proteins that regulate Ca^{2+} transfer also mediate the elevation of mito-Ca^{2+} level in *PINK1* mutant DA neurons. RNAi of IP3R, MCU, or Porin significantly reduced mito-Ca^{2+} level as monitored with mito-GCaMP (Fig. 2*D*). Using *IP3R* and *Porin* mutant alleles, we confirmed the effect of IP3R and Porin on mito-Ca^{2+} level in Miro-OE condition (*SI Appendix*, Fig. S5*D*). The level of mito-GCaMP expression was not affected by the manipulations of the ERMCS components in *PINK1* mutant condition (*SI Appendix*, Fig. S5*E*). Pan-neuronal Porin inhibition (*elav* > *Porin-RNAi*) in WT or *PINK1* mutant condition resulted in lethality, whereas Porin inhibition specifically in DA neurons reduced mito-GCaMP intensity and depolarized MMP (*SI Appendix*, Fig. S6*C*).

These RNAi manipulations did not affect mitochondrial morphology or mass (*SI Appendix*, Fig. S5*F*), and had no obvious effects on basal mito-Ca^{2+} level in DA neurons (*SI Appendix*, Fig. S5*G*) or on DA neuron survival (*SI Appendix*, Fig. S5*H*) in WT background, even in the case of RNAi of MCU, a key importer of mito-Ca^{2+}. These factors seem to be more important in causing the aberrant mito-Ca^{2+} elevation in Miro-OE and *PINK1* mutant conditions, but under normal physiological condition other mechanisms may counterbalance the effect of ERMCS on mito-Ca^{2+} homeostasis. Other mito-Ca^{2+} influx or efflux pathways may compensate for the partial inhibition of MCU under basal condition, for example MCU-independent mito-Ca^{2+} influx pathways or the sodium-calcium exchanger (NCLX) pathway that counters MCU-mediated Ca^{2+} influx. This may explain the lack of effect on basal metabolism and survival of *MCU* null mutants in the mouse (28) and fly (29).

To corroborate these genetic interaction studies, we performed pharmacological studies by inhibiting IP3R with 2-aminoethoxydiphenyl borate (2-APB), or MCU with Ru360. Both drugs were delivered to the fly brain by feeding (13). We found that both drugs effectively rescued the mito-Ca^{2+} level elevation observed in Miro-OE (Fig. 2*E*) and *PINK1* mutant (Fig. 2*F*) DA neurons. Treatment of LRRK2-G2019S OE flies

with 2-APB or Ru360 also rescued mito-Ca^{2+} in DA neurons (*SI Appendix*, Fig. S6*A*). In the case of Ru360, when applied directly to primary neuronal culture after storing at room temperature (RT) for extended time, it also reduced mito-Ca^{2+} level (*SI Appendix*, Fig. S6*B*). Thus, with the caveat that both 2-APB and Ru360 are not exclusively specific for IP3R and MCU and likely affect other proteins and cellular processes, the pharmacological data corroborated the genetic data and together they supported the notion that Ca^{2+} transfer through the ERMCS critically mediates the effect of Miro on mito-Ca^{2+} homeostasis, which is deregulated in two PD models.

Mito-Ca^{2+} Critically Influences Neuronal Mitochondrial Morphology Independently of the Canonical Fission–Fusion Machinery. We next examined the effect of Miro-mediated mito-Ca^{2+} homeostasis on mitochondrial function and the survival of DA neurons in adult flies, which are known to be sensitive to Miro-OE (26). DA neuron loss in adult brain induced by Miro-OE was rescued by RNAi of Porin, IP3R, dMCU, of Marf (Fig. 3 *A* and *B*). Knockdown of Porin, IP3R, dMCU, of Marf alone had no obvious effect on DA neuron number (*SI Appendix*, Fig. S5*H*). Moreover, Miro-OE led to dramatic enlargement of mitochondria in DA neurons (Fig. 3 *C* and *D*), similar to that seen in *PINK1* mutant (26). Surprisingly, promoting mitochondrial fission and disaggregating mitochondria by Drp1-OE (30), had little effect on this mitochondrial enlargement (Fig. 3*B*) or DA neuron loss (Fig. 3*D*). Inhibition of Drp1 by OE of a dominant-negative form (Drp1-DN) also had no obvious effect (*SI Appendix*, Fig. S3*A*). The mitochondrial morphology change and the neurotoxicity associated with Miro-OE are thus unlikely caused by an imbalance in canonical fission/fusion activities. Inhibition of Milton also failed to alter Miro-induced phenotypes (Fig. 3 *B* and *D*), suggesting that the

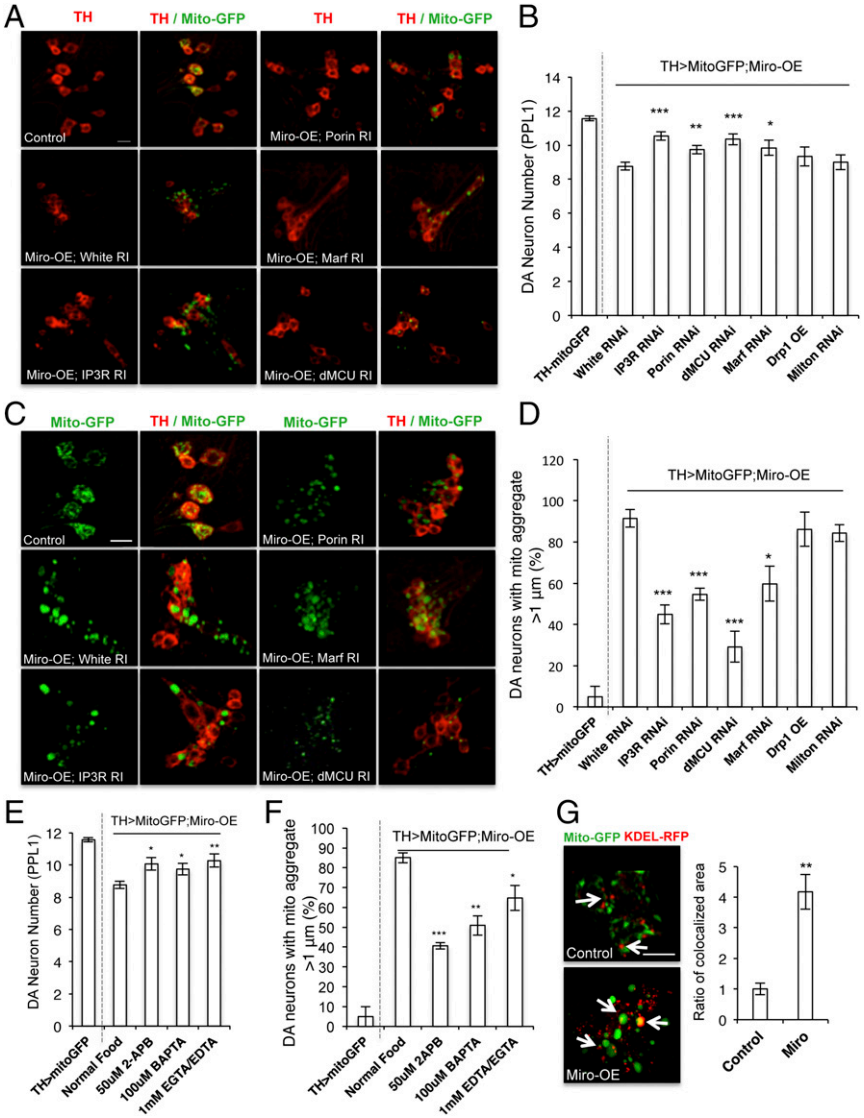

Fig. 3. Mito-Ca^{2+} influx through ERMCS mediates Miro-OE effect on mitochondrial morphology and DA neuron maintenance. (*A* and *B*) Immunostaining of the PPL1 cluster of DA neurons of adult animals (*A*) and data quantification (*B*) showing the effects of ERMCS component RNAi, Milton-RNAi, or Drp1-OE on DA neuron number in Miro-OE condition. (*C* and *D*) Mito-GFP reporter staining in the PPL1 cluster of adult DA neurons (*C*), and data quantification (*D*) showing the effects of ERMCS component RNAi, Milton-RNAi, or Drp1-OE on mitochondrial morphology in Miro-OE condition. (*E* and *F*) Data quantification showing the effects of Ca^{2+} chelation with BAPTA or EGTA/EDTA, and IP3R inhibition with 2-APB, on DA neuron number (*E*) and mitochondrial morphology (*F*) in Miro-OE flies. (*G*) Representative immunostaining and data quantification showing increased mitochondria–ER contact in Miro-OE DA neurons. Arrows point to areas of contact. Error bar: SEM; $*P < 0.05$, $**P < 0.01$, $***P < 0.001$ versus control in one-way ANOVA. $n = 10$. (Scale bars in *A*, *C*, and *G*: 10 µm.)

toxic effects of Miro-OE studied here may not be related to transport.

In contrast, correlating with their effective rescue of Miro-OE–induced DA neuron loss, RNAi of dMCU, and to a lesser extent, RNAi of IP3R and Porin, rescued Miro-OE–induced mitochondrial enlargement (Fig. 3 *C* and *D*). The mitochondrial morphology defect and DA neuron degeneration caused by Miro-OE thus may be associated with enhanced Ca^{2+} influx from the ER and the ensuing mito-Ca^{2+} overload. Consistent with mito-Ca^{2+} overload being causal, pharmacological reduction of Ca^{2+} availability with BAPTA or EDTA/EGTA, or inhibition of IP3R with 2-APB, rescued Miro-OE–induced mitochondrial enlargement and DA neuron loss (Fig. 3 *E* and *F*). Importantly, we observed significantly increased contact between mitochondria and ER in Miro-OE DA neurons than control DA neurons (Fig. 3*G*). Together with our previous biochemical data showing enhancement of IP3R–VDAC physical interaction by Miro-OE (13), these results suggest that Miro promotes mitochondria–ER connectivity in DA neurons.

The function of Miro in mediating Ca^{2+} transfer through the ERMCS is positively regulated by Polo through direct phosphorylation (13). We next tested the role of Polo/Miro signaling in DA neuron maintenance. The DA neuron loss caused by Miro-OE was effectively rescued by Polo-RNAi (*SI Appendix*, Fig. S7*A*). Moreover, OE of Polo-GFP or a constitutively active form of Polo (Polo-CA) resulted in DA neuron loss, which was rescued by Miro-RNAi or the coexpression of a phosphomutant of Miro (Miro-S66A), but not Miro-WT (*SI Appendix*, Fig. S7*A*). Thus, the function of Miro in controlling mitochondrial morphology and DA neuron maintenance through mito-Ca^{2+} homeostasis is regulated by Polo.

Mito-Ca^{2+} Homeostasis Mediated by ERMCS Is Critical for PINK1 Function in DA Neurons. Loss of fly PINK1 function resulted in mitochondrial dysfunction, aberrant mitochondrial morphology, and neuromuscular tissue degeneration (31–33), recapitulating key features of PD. We next tested whether mito-Ca^{2+} homeostasis mediated by ERMCS is relevant to PINK1 function in vivo. Knockdown of Miro, IP3R, and MCU in DA neurons of the adult brain rescued the DA neuron loss (Fig. 4 *A* and *B*) and the mitochondrial enlargement (Fig. 4 *C* and *D*) phenotypes caused by *PINK1* inactivation. Moreover, knockdown of Miro, IP3R, and MCU in *PINK1* mutant muscle tissue restored mitochondrial morphology (*SI Appendix*, Fig. S7*C*) and partially prevented the degeneration of indirect flight muscle, which is manifested as abnormal wing posture (*SI Appendix*, Fig. S7*D*), and these effects are partially correlated with restoration of ATP levels (*SI Appendix*, Fig. S7*B*). Similar genetic manipulation of these genes in a wild-type background had no obvious effects on mitochondrial morphology (*SI Appendix*, Fig. S7*C*), or wing posture (*SI Appendix*, Fig. S7*D*), although the effects on ATP production were variable (*SI Appendix*, Fig. S7*B*), especially in the case of MCU, presumably due to a compensatory response in ATP production as observed in *MCU* knockout mice (34). Together, these results strongly support the critical role of mito-Ca^{2+} homeostasis regulated by Ca^{2+} transfer through the ERMCS in mediating PINK1 function in neuromuscular tissues in an intact animal. Consistent with this notion, we found that ER–mitochondria connectivity is significantly enhanced in *PINK1* mutant DA neurons (Fig. 4*E*), as observed in Miro-OE (Fig. 3*G*). Further supporting this notion, we performed coimmunoprecipitation between IP3R and VDAC, which has been used to detect the strength of ERMCSs (35). We also used proximity ligation assay (36) to assess the extent of ERMCS formation (37). Our results confirmed that ERMCS is enhanced when PINK1 is inhibited (*SI Appendix*, Fig. S8 *A* and *B*). Loss of DA neurons (*SI Appendix*, Fig. S9*A*) and mitochondrial enlargement (*SI Appendix*, Fig. S9*B*) observed in *PINK1* mutant were rescued by

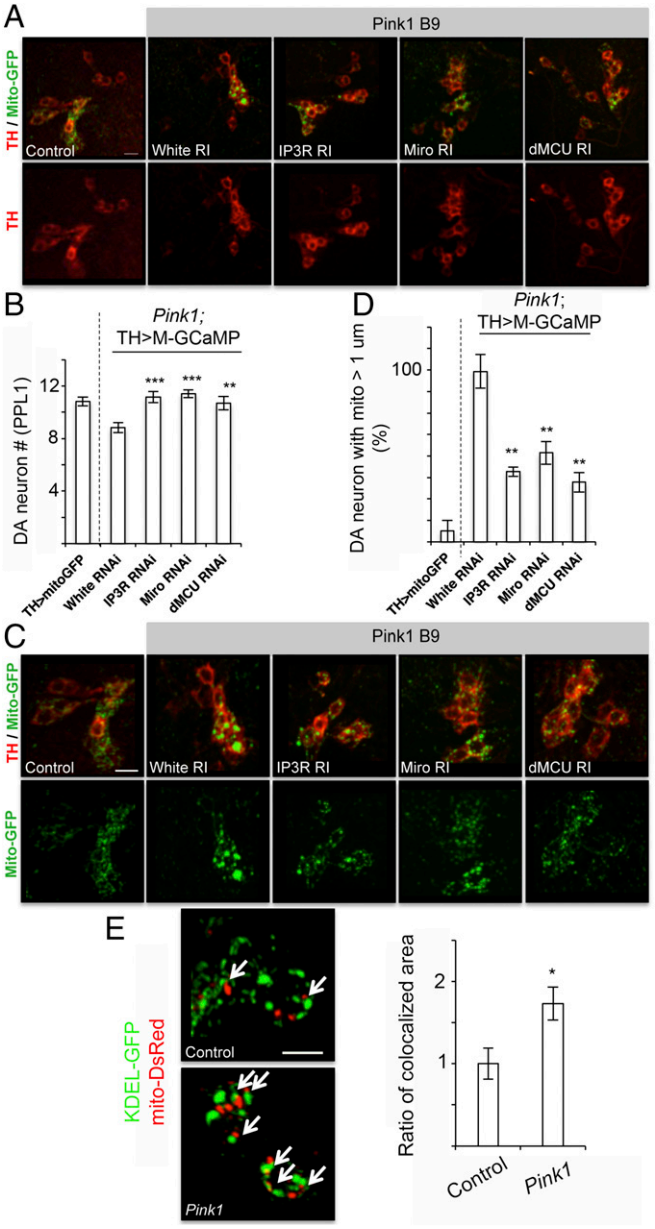

Fig. 4. Pathogenic role of mito-Ca^{2+} homeostasis mediated by ERMCS in *PINK1* PD model. (*A* and *B*) Immunostaining of the PPL1 cluster of DA neurons of adult animals (*A*) and data quantification (*B*) showing the effects of ERMCS component RNAi on DA neuron number in *PINK1* mutant. (*C* and *D*) Mito-GFP reporter staining in the PPL1 cluster of adult DA neurons (*C*) and data quantification (*D*) showing the effects of ERMCS component RNAi on mitochondrial enlargement in *PINK1* mutant. (*E*) Representative immunostaining and quantification of mitochondria–ER colocalization in *PINK1* mutant DA neurons. Arrows point to areas of contact. Error bar: SEM; $*P < 0.05$, $**P < 0.01$, $***P < 0.001$ versus control in one-way ANOVA. $n = 10$. (Scale bars in *A*, *C*, and *E*: 10 μm.)

pharmacological agents that chelate intracellular or extracellular Ca^{2+} (BAPTA or EDTA/EGTA) or block Ca^{2+} transfer through the ERMCS (2-APB or Ru360).

Regulation of Mito-Ca^{2+} Homeostasis by Miro and ERMCS Is Important for Synaptic Morphogenesis at the Neuromuscular Junction. Mitochondrial dysfunction and synaptic aberration precede frank neuronal degeneration and are early pathogenic events. However, the relationship between these pathogenic events is not well

understood. To assess the synaptic effects of mito-Ca^{2+} regulated by Polo/Miro signaling, we used the *Drosophila* larval neuromuscular junction (NMJ) as a model, which offers an accessible system to study synapse development, function, and regulation. Presynaptic (*elav-Gal4*-driven) Miro-OE induced morphological defects manifested as loss of boutons formed on muscle 6/7 of the A3 segment (Fig. 5 *A* and *B*), consistent with Miro being critically needed for synaptic growth (14). This Miro-OE effect was fully rescued by *polo* heterozygosity ($polo^{9/+}$) or Polo-RNAi, but not Polo(CA)-OE (Fig. 5 *A* and *B*). $polo^{9/+}$, Polo-RNAi, or Polo(CA)-OE alone had no discernible effect on NMJ morphology, and muscle fiber size was also not affected. To assess the effect of Miro phosphorylation by Polo on synaptic morphogenesis, we compared NMJ morphology after presynaptic OE of Miro-WT, the phosphomutant Miro-S66A, or the phosphomimetic Miro-S66E. While Miro-WT caused ∼40% reduction in the number of boutons formed on muscle 6/7 of A3, Miro-S66A had no obvious effect. In contrast, Miro-S66E showed a slightly stronger effect than Miro-WT (Fig. 5 *C* and *D*). These results support the importance of phosphorylation by Polo on the synaptic function of Miro.

We next asked whether the proteins controlling the ERMCS and calcium transfer mediate the synaptic effect of Miro. The bouton-loss phenotype induced by Miro-OE was partially rescued by RNAi of IP3R, Porin, or MCU (Fig. 5 *E* and *F*), although the RNAi of IP3R, Porin, or MCU alone had no obvious effect (Fig. 5*F*). The effect of Miro-OE on synaptic morphology was not significantly affected by Milton-RNAi (*SI Appendix*, Fig. S10*A*), suggesting that mitochondrial transport may not be a main determinant of the effect of Miro on synaptic morphogenesis. Consistent with ERMCS-mediating Miro effect at the NMJ by facilitating Ca^{2+} transfer, we observed increased mito-Ca^{2+} in the cell bodies and axons of neurons in the ventral nerve cord that contain motor neurons forming synapses at the NMJ, and this mito-Ca^{2+} elevation was abolished by IP3R-RNAi (*SI Appendix*, Fig. S10 *B* and *C*).

LRRK2 also regulates synaptic structure and function at the NMJ, with OE of both WT and pathogenic LRRK2 causing bouton loss (23). We found that Miro-RNAi effectively rescued the bouton-loss phenotype caused by LRRK2, whereas Miro-OE had an opposite effect (Fig. 5*G*). Pharmacological agents that block Ca^{2+} transfer through the ERMCS (2-APB or Ru360) showed a trend of rescuing LRRK2-G2019S–induced bouton loss, although they did not achieve statistical significance (*SI Appendix*, Fig. S10*D*). By demonstrating the critical roles of mito-Ca^{2+} homeostasis regulators Miro and ERMCS in an in vivo setting that

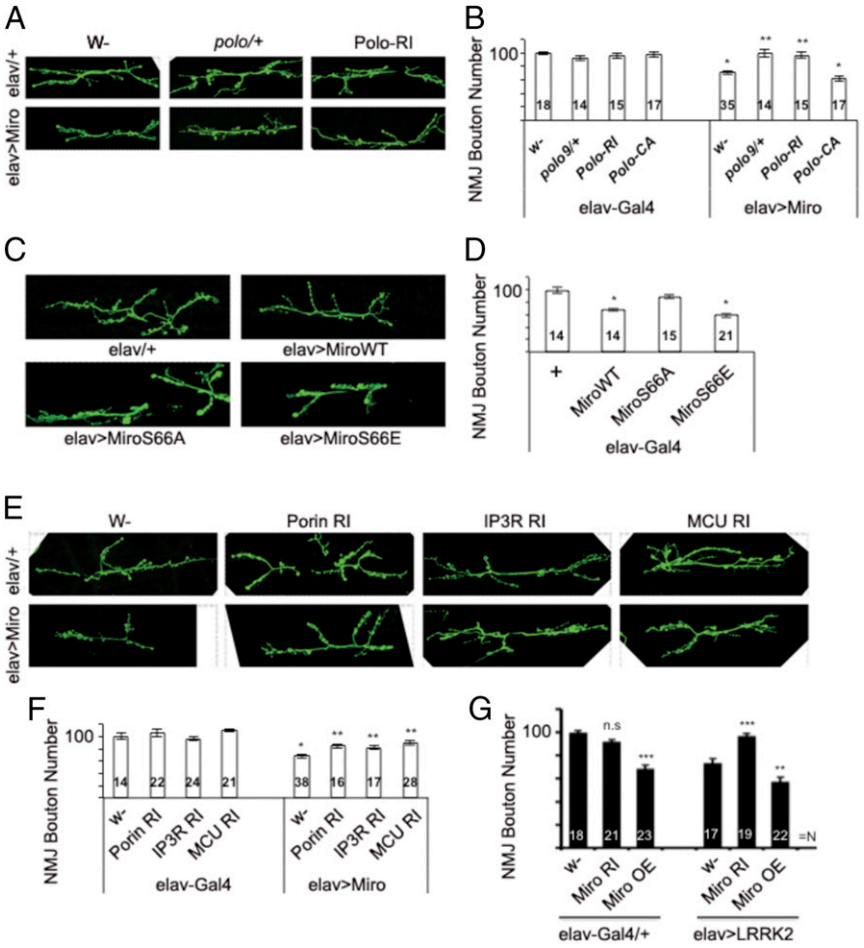

Fig. 5. Effect of Miro-regulated ER–mitochondria Ca^{2+} signaling on NMJ synaptic morphogenesis. (*A* and *B*) Immunostaining of third instar larvae with anti-HRP showing effects of Polo heterozygosity or Polo-RNAi on NMJ morphology (*A*) in wild-type or dMiro-OE condition, and quantification of bouton number (*B*). Green, HRP. *N*, number of animals analyzed. (*C* and *D*) Immunostaining of third instar larvae with anti-HRP showing effects of OE of Miro WT or phosphovariants on NMJ morphology (*C*) and bouton number (*D*). (*E* and *F*) Effects of RNAi of ERMCS components on NMJ morphology (*E*) and bouton number (*F*). (*G*) Effects of Miro-RNAi and Miro-OE on NMJ bouton number in hLRRK2-G2019S OE condition. Error bar: SEM; $*P < 0.05$, $**P < 0.01$, $***P < 0.001$ versus control in one-way ANOVA. n.s, nonsignificant. (Magnification: *A*, 195×; *C* and *E*, 280×.)

assesses synaptic morphogenesis and growth, these studies highlight the broader effect of mito-Ca^{2+} on neuronal health.

Altered Mitochondrial Ca^{2+} Homeostasis Is Critically Involved in PAR-1–Induced Neurodegeneration. We further examined the role of altered mito-Ca^{2+} homeostasis in other models of neurodegeneration. For this purpose, we used the PAR-1 transgenic model. PAR-1 OE causes photoreceptor degeneration in the eye and disruption of synaptic morphogenesis at the NMJ (38, 39). Using the mito-GCaMP reporter expressed in photoreceptor neurons under the control of *GMR-Gal4*, we found that PAR-1 OE induced a dramatic increase of mito-Ca^{2+} (Fig. 6 *A* and *B*). This effect of PAR-1 was blocked by feeding animals with 2-APB (Fig. 6 *A* and *B*) or Ru360 (*SI Appendix*, Fig. S11*A*). 2-APB treatment also modestly reduced the basal mito-Ca^{2+} level in photoreceptor neurons in control animals (Fig. 6 *A* and *B*). Correlating with the rescue of the mito-Ca^{2+} level, the reduction of eye size caused by photoreceptor degeneration in *GMR-Gal4 > PAR-1* flies was partially rescued by 2-APB (Fig. 6*C*) or by IP3R-RNAi (Fig. 6*D*).

At the NMJ, PAR-1 OE led to a reduction of bouton number (39, 40), which was effectively rescued by IP3R-RNAi, whereas IP3R OE significantly enhanced PAR-1 OE effect. RNAi of Porin, MCU, and Miro also effectively rescued the PAR-1 OE effect, although their OE did not exhibit the same enhancing effect as IP3R OE (Fig. 6 *E* and *F*). Miro-mediated mito-Ca^{2+} homeostasis was shown to be important for *Drosophila* central brain neuroblast (NB) function (13). We found that OE of WT but not kinase-dead forms of PAR-1 induced elevation of mito-Ca^{2+} level in NBs (*SI Appendix*, Fig. S11*B*), suggesting that PAR-1 acts in a kinase activity-dependent manner to regulate mito-Ca^{2+} homeostasis. This is correlated with mitochondrial enlargement, which was attenuated by Miro-RNAi (*SI Appendix*, Fig. S11*C*), or pharmacological agents that chelate Ca^{2+} or block Ca^{2+} influx from the ERMCS (*SI Appendix*, Fig. S11*D*). Taken together, these results support the idea that mito-Ca^{2+} homeostasis is highly relevant to PAR-1–induced neurodegeneration.

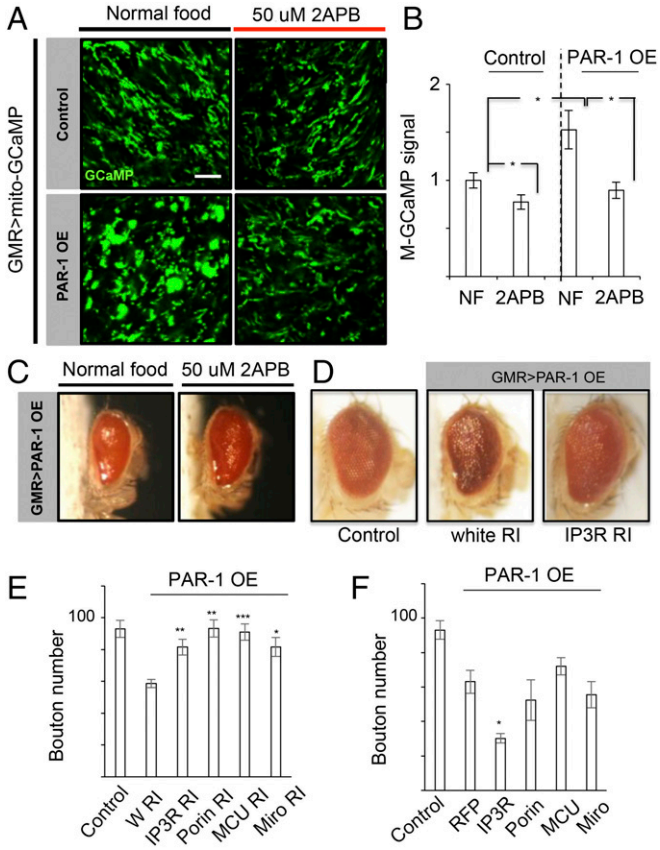

Fig. 6. Mito-Ca^{2+} dyshomeostasis in the *Drosophila* PAR-1 model of neurodegeneration. (*A* and *B*) Mito-GCaMP signals in third instar larval eye discs of control and *GMR-Gal4 > PAR-1* animals grown on normal food or food containing 50 μM 2-APB. Quantification of relative mito-GCaMP signal intensity from *A* is shown in bar graph in *B*. (*C* and *D*) Effects of IP3R inhibition with 2-APB (*C*) or by RNAi (*D*) on the small eye phenotype caused by PAR-1 OE in the photoreceptors. (Magnification: 20×.) (*E* and *F*) Data quantification showing the effects of RNAi (*E*) or OE (*F*) of ERMCS components on NMJ bouton number in *Mhc-Gal4 > PAR-1* condition. Error bar: SEM; $*P < 0.05$, $**P < 0.01$, $***P < 0.001$ versus control in one- and two-way ANOVA. (Scale bars: 5 μm.)

Discussion

As one of the most prominent organelles in eukaryotic cells, mitochondria make intimate contacts with other organelles. The effects of such interorganellar contacts on cellular function are only beginning to be appreciated. Ca^{2+} signaling is intimately linked to mitochondrial physiology and Miro has emerged as a key molecule linking mitochondrial function and Ca^{2+} signaling (41). Previous studies highlighted the role of Miro in directing mitochondrial transport by sensing changes of cytosolic Ca^{2+} levels. The current study demonstrates that Miro also plays critical roles in regulating mito-Ca^{2+} homeostasis in disease-relevant cell types by acting through Ca^{2+} transport at ERMCSs. Although motor neuron studies in *Miro1* null mice did not find an obvious change in mito-Ca^{2+} buffering (42), it is worth pointing out that in mammals there are at least two Miro counterparts. Functional redundancy between Miro1 and Miro2 in mito-Ca^{2+} regulation cannot be ruled out. It is also worth examining mito-Ca^{2+} homeostasis in DA neurons. We further show that PINK1 and LRRK2, which are associated with familial PD, and PAR-1/MARK, which is hyperactivated in AD, regulates mito-Ca^{2+} homeostasis through Miro. Our in vivo studies in *Drosophila* highlighted the significance of balanced mito-Ca^{2+} levels to mitochondrial function and neuronal survival in neurodegenerative disease. Our pharmacological studies provide evidence that manipulating mito-Ca^{2+} homeostasis through ERMCSs may offer a therapeutic avenue.

Mitochondria are dynamic in nature. Neurons are particularly dependent on mitochondrial dynamics, presumably due to their highly polarized morphology and unique bioenergetic needs at strategic locations (24, 43). How mitochondrial number, shape, and distribution are coordinated is a topic of great interest. Studies in yeast (44), flies (26), and mammalian cells (12) demonstrate a strong influence on mitochondrial shape by Miro, although the underlying mechanism is not clear. Our genetic studies in *Drosophila* did not support the canonical fission/fusion regulators and the transport machinery as mediators of Miro effect on mitochondrial morphology. Instead our data implicate the ERMCS and mito-Ca^{2+} in this process. Interestingly, matrix Ca^{2+} has also been suggested as an intrinsic signal controlling mitochondrial transport in neuronal axons (45). These data raise the intriguing possibility that matrix Ca^{2+} may coordinate mitochondrial motility and shape.

It is worth noting that stimulation of fission by Drp1-OE is beneficial in rescuing the mitochondrial morphological and functional defects in *PINK1* mutant (30). PINK1 has been implicated in various aspects of mitochondrial physiology, from biogenesis of respiratory chain components and thus oxidative phosphorylation (OxPhos), to regulation of mitochondrial dynamics and mitophagy. PINK1 has been implicated in mito-Ca^{2+} efflux through NCLX (46), presumably via PKA-mediated phosphorylation of NCLX (47), or through LETM1 (48). Our results suggest that there are increased ERMCSs in *PINK1* mutant DA neurons, likely due to the impaired control of Miro protein abundance, resulting in increased Ca^{2+} transfer from the

ER to mitochondria. Increased ERMCSs in *PINK1* and *Parkin* mutant flies were reported recently in other settings (49), consistent with our findings, although the underlying mechanism and the effect on Ca^{2+} transfer were not studied. MCU but not VDAC was found to mediate the effect of *PINK1* mutation on DA neuron maintenance in zebrafish (50). PINK1 thus plays a multifaceted role in controlling mito-Ca^{2+} homeostasis. The fact that manipulation of mito-Ca^{2+} is beneficial in *PINK1* mutant condition suggests that mito-Ca^{2+} homeostasis is mechanistically or functionally connected to those other aspects of PINK1 function in mitochondrial physiology.

Our results further support the Miro signaling pathway as an important regulator of mito-Ca^{2+} homeostasis mediated by ERMCS in neurons. Despite detailed biophysical studies of mito-Ca^{2+} uptake, little is known about how this process is regulated to meet the unique physiological needs of distinct cell types in a multicellular organism. We show that PINK1/Miro signaling critically regulates mito-Ca^{2+} influx through the ERMCS. This mechanism may act independently or in concert with the PINK1 effect on mito-Ca^{2+} efflux via NCLX (46) or LETM1 (48). Our studies in the LRRK2-G2019S PD model and the PAR-1 model indicate that increased mito-Ca^{2+} is broadly involved in neurodegeneration. It will be interesting to test how the various disease gene products impinge on Miro and components of the ERMCS to alter ER–mitochondria communication. It is also worth pointing out that, given the important role of mito-Ca^{2+} to OxPhos, decreased Ca^{2+} influx from ER to mitochondria due to weakening of the ERMCS may also lead to mitochondrial dysfunction and disease, reminiscent of the situations where loss and gain of Miro function are both detrimental to NSCs (13).

In *Drosophila* and mammalian NSCs, Miro is localized to ERMCSs in a Polo kinase-regulated fashion (13). Intriguingly, like *PINK1* mutations, dysregulation of PLKs has been implicated in PD (51). Given that Miro-OE–induced cell death involves Ca^{2+} overload, mitochondrial dysfunction, oxidative stress, ER stress, and caspase 3 activation (13), key features broadly implicated in neurodegenerative disease, it would be interesting to test in various other disease conditions whether disease signaling pathways converge on PLK/Miro, and whether pharmacological intervention of PLK/Miro signaling may offer therapeutic benefits. It is important to note that to achieve therapeutic benefits, the expression level or activity of Miro needs to be tuned to an appropriate range, as complete inhibition of Miro may cause neurodegeneration (42, 52). The fact that Miro is up-regulated in disease settings suggests that it might be possible to find a therapeutic window.

Materials and Methods

***Drosophila* Genetics.** Fly culture and crosses were performed according to standard procedures and raised at indicated temperatures. *UAS-dMiro-WT*, *UAS-dMiro-S66A*, and *UAS-dMiro-S66E* Tg flies were described before (13). All other commonly used stocks were requested (*SI Appendix*) or obtained from the Bloomington *Drosophila* Stock Center.

Pharmacological Treatment. Drug treatment experiments were performed essentially as described (13). 2-APB (Sigma), Ru360 (Calbiochem), EDTA/EGTA (Sigma), $CaCl_2$ (Sigma), and BAPTA (Life Technologies) dissolved in 0.5% DMSO were mixed in fly food at the indicated final concentrations (50 μM 2-APB, 2 μM Ru360, 1 mM EDTA/EGTA, 10 mM $CaCl_2$, and 100 μM BAPTA). A total of 0.5% DMSO alone was used as vehicle control. Flies were raised on the drug-containing food at 29 °C. Brains of third instar larva were dissected in 1× PBS and placed on glass slides for live imaging.

Immunohistochemistry and Imaging. For adult brain DA neuron immunostaining, brains were dissected in Schneider's medium (Invitrogen) and fixed with 4% formaldehyde in PBS buffer for 45 min at RT. Analysis of the *Drosophila* NMJ of third instar larvae was performed essentially as described (40).

The DA-neuron specific *TH-Gal4* driver was used to express *UAS-mito-GCaMP* (expressing GCaMP fused with an N-terminal mitochondrial targeting sequence) and analyzed at either the third instar larvae or adult fly stage raised at 29 °C. Brains were dissected in 1× PBS and immediately placed on the glass slides for live imaging. See *SI Appendix* for details.

Measurement of ER–Mitochondria Contact. The *TH-Gal4* driver was used to drive the expression of *UAS-mito-GFP* and *UAS-KDEL-RFP*, or *UAS-mito-DsRed* and *UAS-KDEL-GFP* reporter combinations in DA neurons of adult flies raised at 29 °C. The mito-GFP/mito-RFP and KDEL-RFP/KDEL-GFP reporter combinations were used to label mitochondria and ER, respectively. Fly brains were dissected in 1× PBS and immediately placed on the glass coverslips for live imaging. Images were taken with a Leica TCS SP5 AOBS confocal microscope equipped with a laser scanner and a 40× oil-immersion objective. Areas of mitochondria and ER colocalization within a square of 15 μm × 15 μm were measured using ImageJ and the values were summed up. Multiple squares were measured and the values averaged. Averaged values from *PINK1* mutant or *Miro-OE* DA neurons were normalized with the averaged colocalization area in control DA neurons.

ACKNOWLEDGMENTS. We thank members of the B.L. laboratory for discussions and help; and Drs. I. Bezprozvanny, Serge Birman, B. T. Grillo-Hill, J. K. Chung, S. Davies, D. M. Glover, M. Guo, G. Hassan, Y. N. Jan, F. Kawasaki, J. Lipsick, L. Luo, J. Nambu, W. M. Saxton, D. Smith, D. Walker, A. Whitworth, and K. Zinsmaier as well as the Vienna *Drosophila* Resource Center and the Bloomington Stock Center for fly stocks and reagents.

1. Chan DC (2006) Mitochondria: Dynamic organelles in disease, aging, and development. *Cell* 125:1241–1252.
2. Pchitskaya E, Popugaeva E, Bezprozvanny I (2018) Calcium signaling and molecular mechanisms underlying neurodegenerative diseases. *Cell Calcium* 70:87–94.
3. Chan CS, Gertler TS, Surmeier DJ (2009) Calcium homeostasis, selective vulnerability and Parkinson's disease. *Trends Neurosci* 32:249–256.
4. Area-Gomez E, Schon EA (2017) On the pathogenesis of Alzheimer's disease: The MAM hypothesis. *FASEB J* 31:864–867.
5. Mattson MP (2010) ER calcium and Alzheimer's disease: In a state of flux. *Sci Signal* 3: pe10.
6. Area-Gomez E, Schon EA (2016) Mitochondria-associated ER membranes and Alzheimer disease. *Curr Opin Genet Dev* 38:90–96.
7. Popugaeva E, Pchitskaya E, Bezprozvanny I (2017) Dysregulation of neuronal calcium homeostasis in Alzheimer's disease–A therapeutic opportunity? *Biochem Biophys Res Commun* 483:998–1004.
8. Calì T, Ottolini D, Negro A, Brini M (2013) Enhanced parkin levels favor ER-mitochondria crosstalk and guarantee Ca(2+) transfer to sustain cell bioenergetics. *Biochim Biophys Acta* 1832:495–508.
9. Gautier CA, et al. (2016) The endoplasmic reticulum-mitochondria interface is perturbed in PARK2 knockout mice and patients with PARK2 mutations. *Hum Mol Genet* 25:2972–2984.
10. Rizzuto R, Brini M, Murgia M, Pozzan T (1993) Microdomains with high Ca2+ close to IP3-sensitive channels that are sensed by neighboring mitochondria. *Science* 262: 744–747.
11. Rizzuto R, De Stefani D, Raffaello A, Mammucari C (2012) Mitochondria as sensors and regulators of calcium signalling. *Nat Rev Mol Cell Biol* 13:566–578.
12. Fransson A, Ruusala A, Aspenström P (2003) Atypical Rho GTPases have roles in mitochondrial homeostasis and apoptosis. *J Biol Chem* 278:6495–6502.
13. Lee S, et al. (2016) Polo kinase phosphorylates Miro to control ER-mitochondria contact sites and mitochondrial Ca(2+) homeostasis in neural stem cell development. *Dev Cell* 37:174–189.
14. Guo X, et al. (2005) The GTPase dMiro is required for axonal transport of mitochondria to Drosophila synapses. *Neuron* 47:379–393.
15. Glater EE, Megeath LJ, Stowers RS, Schwarz TL (2006) Axonal transport of mitochondria requires milton to recruit kinesin heavy chain and is light chain independent. *J Cell Biol* 173:545–557.
16. Kornmann B, Osman C, Walter P (2011) The conserved GTPase Gem1 regulates endoplasmic reticulum-mitochondria connections. *Proc Natl Acad Sci USA* 108: 14151–14156.
17. Lutas A, Wahlmark CJ, Acharjee S, Kawasaki F (2012) Genetic analysis in Drosophila reveals a role for the mitochondrial protein p32 in synaptic transmission. *G3 (Bethesda)* 2:59–69.
18. Sarkar AR, et al. (2016) A ratiometric two-photon probe for quantitative imaging of mitochondrial pH values. *Chem Sci (Camb)* 7:766–773.
19. Nakai J, Ohkura M, Imoto K (2001) A high signal-to-noise Ca(2+) probe composed of a single green fluorescent protein. *Nat Biotechnol* 19:137–141.
20. Kalbácová M, Vrbacký M, Drahota Z, Melková Z (2003) Comparison of the effect of mitochondrial inhibitors on mitochondrial membrane potential in two different cell lines using flow cytometry and spectrofluorometry. *Cytometry A* 52:110–116.
21. Williams CC, Jan CH, Weissman JS (2014) Targeting and plasticity of mitochondrial proteins revealed by proximity-specific ribosome profiling. *Science* 346:748–751.

22. Lee KS, et al. (2013) Roles of PINK1, mTORC2, and mitochondria in preserving brain tumor-forming stem cells in a noncanonical Notch signaling pathway. *Genes Dev* 27: 2642–2647.
23. Lee S, Liu HP, Lin WY, Guo H, Lu B (2010) LRRK2 kinase regulates synaptic morphology through distinct substrates at the presynaptic and postsynaptic compartments of the Drosophila neuromuscular junction. *J Neurosci* 30:16959–16969.
24. Sheng ZH, Cai Q (2012) Mitochondrial transport in neurons: Impact on synaptic homeostasis and neurodegeneration. *Nat Rev Neurosci* 13:77–93.
25. Wang X, et al. (2011) PINK1 and Parkin target Miro for phosphorylation and degradation to arrest mitochondrial motility. *Cell* 147:893–906.
26. Liu S, et al. (2012) Parkinson's disease-associated kinase PINK1 regulates Miro protein level and axonal transport of mitochondria. *PLoS Genet* 8:e1002537.
27. Iijima-Ando K, et al. (2012) Loss of axonal mitochondria promotes tau-mediated neurodegeneration and Alzheimer's disease-related tau phosphorylation via PAR-1. *PLoS Genet* 8:e1002918.
28. Pan X, et al. (2013) The physiological role of mitochondrial calcium revealed by mice lacking the mitochondrial calcium uniporter. *Nat Cell Biol* 15:1464–1472.
29. Choi S, et al. (2017) Mitochondrial calcium uniporter in *Drosophila* transfers calcium between the endoplasmic reticulum and mitochondria in oxidative stress-induced cell death. *J Biol Chem* 292:14473–14485.
30. Yang Y, et al. (2008) Pink1 regulates mitochondrial dynamics through interaction with the fission/fusion machinery. *Proc Natl Acad Sci USA* 105:7070–7075.
31. Yang Y, et al. (2006) Mitochondrial pathology and muscle and dopaminergic neuron degeneration caused by inactivation of Drosophila Pink1 is rescued by Parkin. *Proc Natl Acad Sci USA* 103:10793–10798.
32. Park J, et al. (2006) Mitochondrial dysfunction in Drosophila PINK1 mutants is complemented by parkin. *Nature* 441:1157–1161.
33. Clark IE, et al. (2006) Drosophila pink1 is required for mitochondrial function and interacts genetically with parkin. *Nature* 441:1162–1166.
34. Nichols M, et al. (2017) Global ablation of the mitochondrial calcium uniporter increases glycolysis in cortical neurons subjected to energetic stressors. *J Cereb Blood Flow Metab* 37:3027–3041.
35. Betz C, et al. (2013) Feature article: mTOR complex 2-Akt signaling at mitochondria-associated endoplasmic reticulum membranes (MAM) regulates mitochondrial physiology. *Proc Natl Acad Sci USA* 110:12526–12534.
36. Lambert TD, Howard J, Plant A, Soffe S, Roberts A (2004) Mechanisms and significance of reduced activity and responsiveness in resting frog tadpoles. *J Exp Biol* 207: 1113–1125.
37. Hedskog L, et al. (2013) Modulation of the endoplasmic reticulum-mitochondria interface in Alzheimer's disease and related models. *Proc Natl Acad Sci USA* 110: 7916–7921.
38. Nishimura I, Yang Y, Lu B (2004) PAR-1 kinase plays an initiator role in a temporally ordered phosphorylation process that confers tau toxicity in Drosophila. *Cell* 116: 671–682.
39. Zhang Y, et al. (2007) PAR-1 kinase phosphorylates Dlg and regulates its postsynaptic targeting at the Drosophila neuromuscular junction. *Neuron* 53:201–215.
40. Lee S, Wang JW, Yu W, Lu B (2012) Phospho-dependent ubiquitination and degradation of PAR-1 regulates synaptic morphology and tau-mediated Aβ toxicity in Drosophila. *Nat Commun* 3:1312.
41. Lee KS, Lu B (2014) The myriad roles of Miro in the nervous system: Axonal transport of mitochondria and beyond. *Front Cell Neurosci* 8:330.
42. Nguyen TT, et al. (2014) Loss of Miro1-directed mitochondrial movement results in a novel murine model for neuron disease. *Proc Natl Acad Sci USA* 111:E3631–E3640.
43. Saxton WM, Hollenbeck PJ (2012) The axonal transport of mitochondria. *J Cell Sci* 125: 2095–2104.
44. Frederick RL, McCaffery JM, Cunningham KW, Okamoto K, Shaw JM (2004) Yeast Miro GTPase, Gem1p, regulates mitochondrial morphology via a novel pathway. *J Cell Biol* 167:87–98.
45. Chang KT, Niescier RF, Min KT (2011) Mitochondrial matrix Ca2+ as an intrinsic signal regulating mitochondrial motility in axons. *Proc Natl Acad Sci USA* 108:15456–15461.
46. Gandhi S, et al. (2009) PINK1-associated Parkinson's disease is caused by neuronal vulnerability to calcium-induced cell death. *Mol Cell* 33:627–638.
47. Kostic M, et al. (2015) PKA phosphorylation of NCLX reverses mitochondrial calcium overload and Depolarization, promoting survival of PINK1-deficient dopaminergic neurons. *Cell Rep* 13:376–386.
48. Huang E, et al. (2017) PINK1-mediated phosphorylation of LETM1 regulates mitochondrial calcium transport and protects neurons against mitochondrial stress. *Nat Commun* 8:1399.
49. Valadas JS, et al. (2018) ER lipid defects in neuropeptidergic neurons impair sleep patterns in Parkinson's disease. *Neuron* 98:1155–1169.e6.
50. Soman S, et al. (2017) Inhibition of the mitochondrial calcium uniporter rescues dopaminergic neurons in pink1$^{-/-}$ zebrafish. *Eur J Neurosci* 45:528–535.
51. Mbefo MK, et al. (2010) Phosphorylation of synucleins by members of the Polo-like kinase family. *J Biol Chem* 285:2807–2822.
52. López-Doménech G, et al. (2016) Loss of dendritic complexity precedes neurodegeneration in a mouse model with disrupted mitochondrial distribution in mature dendrites. *Cell Rep* 17:317–327.